
Manifold Preserving Adversarial Learning

Ousmane Amadou Dia*

Element AI

ousmane@elementai.com

Elnaz Barshan

Element AI

elnaz.barshan@elementai.com

Reza Babanezhad

University of British Columbia

babanezhad@gmail.com

Abstract

How to generate semantically meaningful and structurally sound adversarial examples? We propose to answer this question by restricting the search for adversaries in the true data manifold. To this end, we introduce a stochastic variational inference method to learn the data manifold, in the presence of continuous latent variables with intractable posterior distributions, without requiring an a-priori form for the data underlying distribution. We then propose a manifold perturbation strategy that ensures the cases we perturb remain in the manifold of the original examples and thereby generate the adversaries. We evaluate our approach on a number of image and text datasets. Our results show the effectiveness of our approach in producing coherent, and realistic-looking adversaries that can evade strong defenses known to be resilient to traditional adversarial attacks.

1 Introduction

Recent developments in adversarial machine learning [1, 2] have cast serious concerns on the robustness of deep learning models. Although many defense mechanisms [3, 4, 5, 6] have been proposed to alleviate the security risks faced by these models, very few stand resilient to attacks [1, 7]. This suggests the need to probe the models even more to discover their vulnerabilities. Adversarial attacks aim in general at manipulating images or text data with tiny targeted nuisances so as to deceive a classifier into making incorrect predictions. For images, the adversarial examples are generated to be identical to the inputs albeit the precise locations of some details in the true images might still not be preserved. We reckon that exact locations of fine details are not necessarily relevant for perceptual recognition. For text, however, this is not always the case. Indeed, slight perturbations to text can alter its readability and corrupt its meaning. Being able to generate coherent and informative adversarial text implies the need for the adversaries to be grammatically and linguistically sound. That is, the text adversaries need to retain the structure and convey ideally the meaning of the original inputs. We posit that the reason existing approaches fail to enforce such requirements both for images and text is because the adversaries they create do not necessarily lie within the manifold of the true cases. This could be attributed to the difficulty to characterize such manifold and to perturbing the inputs along suboptimal gradient directions [8, 9, 10].

In this study, we explore a novel approach based on the manifold invariance property, which we formalize below, to generate coherent, diverse, and meaningful adversaries in the image and text domains. We especially require the adversaries to reflect the structure and semantics of the true inputs; that is *their distributions should match*. To intuitively introduce our framework, we first decompose the noise-based adversarial learning problem into: (1) manifold learning where we develop a novel

*Correspondence to Ousmane Amadou Dia .

variational inference technique to project high-dimensional data into a low dense representation that faithfully characterizes its distribution, and (2) manifold perturbation under the *manifold invariance* constraint where we describe a simple yet efficient perturbation strategy that ensures cases we perturb remain in the manifold of the true examples. We subsequently illustrate how the rich latent structure exposed in the manifold can be leveraged as a source of knowledge upon which adversarial constraints can be imposed concomitantly with learning the manifold. We apply our approach to both images and text data in a black-box setting to generate adversaries that are structurally and semantically sound, and perceptually similar to the real inputs. Before we proceed, we formalize the invariance concept:

Definition 1.1. Manifold Invariance. Let (\mathcal{X}, d) be a metric space and $h: \mathcal{X} \mapsto \mathcal{X}$ a homeomorphism. Given $u \in \mathcal{X}$, a neighborhood \mathcal{U} of u is *invariant* or *stable* under h if:

$$\mathcal{U} = \left\{ v \in \mathcal{X} : \lim_{n \rightarrow \infty} d(h^n(u), h^n(v)) = 0 \right\}$$

Definition 1.1 stipulates that u and any point $v \in \mathcal{U}$ remain close, in distance, as the number of mappings n increase. To see how Definition 1.1 can be enforced in an adversarial setting, notice first that all the points $v \in \mathcal{U}$ are similar to u up to a constant ϵ by the limit convergence². Thus, we only need find one point v that fools a classifier. However, characterizing the topology of \mathcal{U} is challenging, *much more so in the latent \mathcal{Z} space we operate*. Hence, we consider two transformations $h_1: \mathcal{X} \mapsto \mathcal{Z}$ and $h_2: \mathcal{X} \mapsto \mathcal{Z}$ parameterized respectively by ω_1 and ω_2 and use h_2 to find points that lie in the neighborhood \mathcal{U} of $h_1(u)$ in \mathcal{Z} . We map them back to \mathcal{X} and select the sample that induces adversariality. We define our adversarial learning objective as:

Definition 1.2. Adversarial Learning. Let (\mathcal{X}, d) , (\mathcal{Z}, d) be metric spaces, g a black-box classifier, and $\phi: \mathcal{Z} \mapsto \mathcal{X}$ a mapping function. Let $\tilde{h}_1 = \phi \circ h_1$ and $\tilde{h}_2 = \phi \circ h_2$. We want to learn ω_1 , ω_2 , and ϕ such that $\lim_{n \rightarrow \infty} d(h_1 \circ \tilde{h}_1^n(u), h_2 \circ \tilde{h}_2^n(u)) = 0$ and $g(u) \neq g(\tilde{h}_2^n(u))$ with the f -divergence between ω_1 and ω_2 : $\mathcal{D}_f(\omega_1 \parallel \omega_2) \rightarrow 0$.

The main contributions of our work are thus: we propose (1) a stochastic variational inference method for manifold learning in the presence of continuous latent variables with intractable and implicit posterior distributions, (2) an intuitive manifold perturbation strategy that guarantees perturbed elements of a manifold remain within it, (3) a natural way to generate adversarial examples by ensuring they follow probability distributions similar to the inputs, and (4) illustration on images and text, as well as the empirical validation.

2 Problem Setup & Architecture

Consider \mathcal{D} a dataset of training examples, \mathcal{Y} their corresponding classes, and g a black-box classifier. We want to generate adversarial examples of the true cases. Essentially, for $x \in \mathcal{D}$ and its class y , we want its adversary x' to come from a distribution similar to \mathcal{P}_x of x . In particular, we require x' to be the nearest such instance to x in the manifold that defines the data distribution \mathcal{P}_x and subject to adversariality. By “nearest”, we mean the instance x' must portray similar high-level structure and semantic features as x . Therefore, we ask ourselves the following questions:

1. *How to learn the manifold \mathcal{M} that best characterizes the structure and semantics of \mathcal{D} ?*
2. *How to perturb the elements of \mathcal{M} such that the perturbed elements also stay in \mathcal{M} ?*
3. *How to guide the perturbation process to generate coherent and informative adversaries?*

To address these questions, and setting Definition 1.2 as our guiding principle, we propose as framework the architecture depicted in Figure 1. Our framework is essentially a variational auto-encoder. The encoder is reshaped to faithfully model the true underlying distribution of \mathcal{D} instead of its relaxed approximation [11]. This is achieved by using a more subtle inference mechanism that optimizes both for uncertainty and guarantees easy sampling at inference time. The decoder on the other hand acts as a generative model for crafting adversaries, and a proxy for creating latent targets in the z -space in order to optimize the encoder; a process we refer to as inversion [12] and illustrate in Figure 2. We discuss both features in detail in section 4.1.

²The limit convergence in Definition 1.1 can be re-written as follows: $\forall \epsilon > 0, \exists n_0 : \forall n \geq n_0, d(h^n(u), h^n(v)) < \epsilon$.

Unlike most perturbation-based approaches [13, 14] that search for adversaries in the input space of \mathcal{D} , we leverage the dense representation of the z -space of \mathcal{D} ; the intuition being that *the z -space captures well the structure and semantics of \mathcal{D}* . Thus, rather than finding the adversary of a given x in \mathcal{D} , we learn to perturb its latent code z in a way that the perturbed version z' and z lie in the same manifold space defined by the distribution \mathcal{P}_x . Then, using our decoder g_ϕ , we construct x' . By learning to efficiently perturb the manifold of \mathcal{D} , and then mapping elements of this low-dimensional space back to the input space, we control simultaneously the perturbations we inject to the adversarial cases thereby ensuring the adversaries are similar to the inputs in structure and semantics.

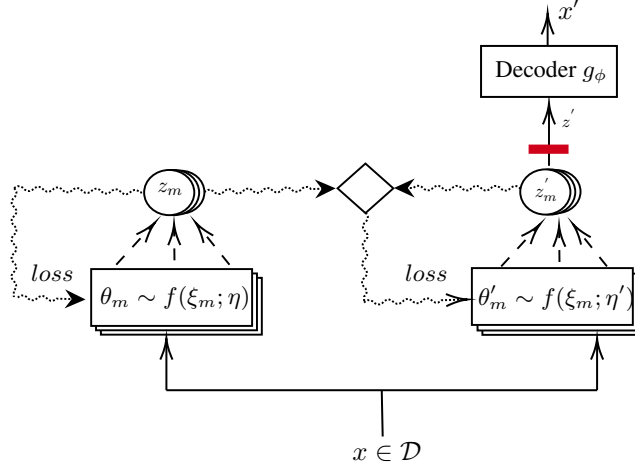


Figure 1: Model Architecture. The model instances θ_m and θ'_m are generated from the networks f_η and $f_{\eta'}$ and used to sample z_m and z'_m given an input x . x' is generated from posterior sampling of a z' (in red) using $\{z'_m\}_m$ passed to the decoder g_ϕ . Undulated lines stand for inner gradient updates.

3 Technical Background

Manifold Learning - To uncover structure in some high dimensional data \mathcal{D} and understand its meta-properties, it is common practice to project \mathcal{D} down to a low dimensional subspace where explanatory hidden features may become apparent. Manifold learning is based on the assumption that the data of interest lies on or near lower dimensional manifolds in its embedding space. In the variational auto-encoder (VAE) [11] setting, the datapoints $x_n \in \mathcal{D}$ are modeled via a decoder $x_n|z_n \sim p_\phi(x_n|z_n)$ with a prior $p(z)$ placed on the latent codes z_n . To learn the parameters ϕ , one typically maximizes a variational approximation to the empirical expected log-likelihood, $1/N \sum_{n=1}^N \log p_\phi(x_n)$, called evidence lower bound (ELBO) and defined by:

$$\mathcal{L}_e(\phi, \psi; x) = \mathbb{E}_{z|x; \psi} \log \left[\frac{p(x|z; \phi)p(z)}{q(z|x; \psi)} \right] = -\mathcal{D}_{KL}(q(z|x; \psi) \| p(z|x; \phi)) + \log p(x; \phi). \quad (1)$$

To evaluate the objective \mathcal{L}_e , we require the ability to sample efficiently from $q(z|x; \psi)$, the encoder distribution which approximates the posterior inference $p(z|x; \phi)$. Specifically, we need a closed and differentiable form for q_ψ in order to evaluate the expectation. The reparameterization trick [11] provides a simple way to rewrite the expectation $\mathbb{E}_{z|x; \psi}$ such that the Monte Carlo estimate of \mathcal{L}_e is differentiable w.r.t ψ . More formally, under some mild differentiability conditions, the random variable $z \sim q_\psi(z|x)$ can be reparameterized using a differentiable transformation $g_\psi(\epsilon, x)$ of an auxiliary noise variable ϵ :

$$z = g_\psi(\epsilon, x) \text{ with } \epsilon \sim p(\epsilon),$$

where the prior $p(\epsilon)$ is generally confined to a *family of simple and tractable distributions* like a Gaussian distribution.

Stein Variational Gradient Descent (SVGD) [15] is a recently proposed nonparametric variational inference method. SVGD combines the strengths of MCMC sampling and variational inference. Unlike variational bayes in VAEs [11], SVGD does not confine the family of approximate distributions within simple or tractable parametric distributions whilst remaining an efficient algorithm. Its update rule is deterministic and leverages the gradient of the target distribution thereby allowing faster

convergence than typical MCMC samplers. SVGD does not require many iterations for the Markov chain to stabilize to its steady state distribution. To obtain M samples from a target distribution $p(\theta)$, SVGD initially maintains M particles $\Theta = \{\theta_m\}_{m=1}^M$ sampled from a simple distribution. Henceforward, we shall consider these particles as instances of model parameters. At iteration t , each particle $\theta \in \Theta$ is updated using the following rule:

$$\theta_{t+1} \leftarrow \theta_t + \epsilon_t \tau(\theta_t) \text{ where } \tau(\theta_t) = \frac{1}{M} \sum_{j=1}^M \left[k(\theta_t^j, \theta_t) \nabla_{\theta_t^j} \log p(\theta_t^j) + \nabla_{\theta_t^j} k(\theta_t^j, \theta_t) \right]. \quad (2)$$

where ϵ_t is a step-size and $k(\cdot, \cdot)$ is a positive-definite kernel. In eq. (2), each particle that gets updated consults first with other particles by asking their gradients, and consequently determines its own update direction. The importance of the other particles is weighted according to the distance measure $k(\cdot, \cdot)$. Closer particles are given higher consideration than those lying further away. The last term $\nabla_{\theta_t^j} k(\theta_t^j, \theta_t)$ is a regularizer that acts as a repulsive force between the particles to prevent them from collapsing into one big particle. The resulting particles can thus be used to approximate the predictive posterior distribution over the dataset \mathcal{D} :

$$p(z|x, \mathcal{D}) = \int p(z|x, \theta) p(\theta|\mathcal{D}) d\theta \approx \frac{1}{M} \sum_{m=1}^M p(z|x, \theta^m) \text{ where } \theta^m \sim p(\theta|\mathcal{D}) \text{ and } z \in \mathcal{Z}. \quad (3)$$

4 Proposed Method

In this section, we first describe a novel stochastic variational inference method to learn the manifold of \mathcal{D} that we denote \mathcal{M} . We want \mathcal{M} to best elicit the structure and semantics of \mathcal{D} with minimal assumptions about the probability distribution of \mathcal{D} . Then, by learning parameterized transformations \mathcal{M} is *invariant* to, we learn to perturb \mathcal{M} , and simultaneously to generate adversarial examples.

4.1 Implicit Manifold Learning

Manifold learning is based on the assumption that the data one attempts to learn lies on or near lower dimensional manifolds in its embedding space. There exist many manifold learning techniques. Of practical interest to us are the VAEs.

As described in section 3, it is customary to optimize the ELBO in eq. (1) when modeling VAEs due to the intractability of the likelihood objective. Moreover, we need a closed and differentiable form for the encoder q_ψ . This is achieved by reparameterizing the encoder q_ψ using a differentiable transformation conditioned on some Gaussian noise. The issue with using a Gaussian prior as distribution for the auxiliary noise is that it leads to uninformative latent codes [16]; which can consequently lead to learning a manifold that characterizes poorly the structure of the data.

Thus, rather than optimizing the ELBO explicitly, [17] minimize the divergence $\mathcal{D}_{KL}(q(z|x; \psi) \| p(z|x; \phi))$. For an instance $x \in \mathcal{D}$, they draw M latent codes by means of a *recognition network* and update them via SVGD. Here, we focus on the \mathcal{D}_{KL} term as well. Similar to [17], we make use of a recognition network to sample model instances that generate these codes during training and inference. In contrast to [17], we generate the latent codes using the sampled model instances or particles and not from directly applying dropout noise on the recognition network.

To start, let $\Theta = \{\theta_m\}_{m=1}^M$ be a set of particles. We aim to leverage these particles to project \mathcal{D} in some latent space \mathcal{Z} . This projection inherently induces uncertainty we ought to capture in order to learn the manifold of \mathcal{D} efficiently. Bayesian methods provide a principled way to model uncertainty through the posterior distribution over model parameters. Thus, we let every particle θ_m define the weights and biases of a Bayesian neural network. For large M , generating the particles can be computationally prohibitive because of the memory footprint. Furthermore, the need to generate them during inference for each test example is undesirable. To remedy this, we train a recognition network $f(\cdot; \eta)$ parameterized by η that takes as input some noise $\xi_m \sim \mathcal{N}(0, I)$ and outputs $\theta_m = f(\xi_m; \eta)$. The parameters η are explicitly updated through a small number of gradient steps in order to produce good generalization performance for the particles. If we denote by η^j the parameters of f at iteration j , we get η^{j+1} by proceeding as follows:

$$\eta^{j+1} \leftarrow \underset{\eta}{\operatorname{argmin}} \sum_{m=1}^M \underbrace{\| f(\xi_m; \eta^j) - \theta_m^{j+1} \|_2^2}_{\theta_m^j} \text{ where } \theta_m^{j+1} \leftarrow \theta_m^j + \epsilon \tau(\theta_m^j) \quad (4)$$

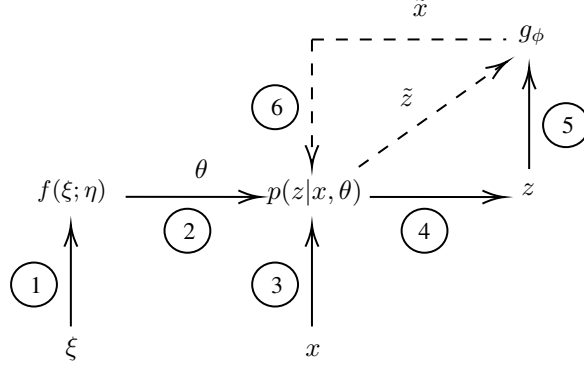


Figure 2: Inversion. During one inner gradient update, we sample some noise ξ that we feed to $f(\cdot; \eta)$ to generate one particle θ . From an example x , we obtain $z \sim p(z|x, \theta)$ that we pass to g_ϕ to get the reconstruction \tilde{x} . Then, \tilde{x} we sample again $\tilde{z} \sim p(z|\tilde{x}, \theta)$. Now, \tilde{z} becomes the target of z . During next update, \tilde{z} becomes the prediction, and we repeat this process to generate a target for \tilde{z} .

with τ is defined in eq. (2). In the following, we shall use $\text{SVGD}_\tau(\Theta)$ to denote one application of this update to Θ .

To apply SVGD_τ , we need to evaluate τ which depends on the posterior $p(z|x, \mathcal{D})$ in eq. (3). Computing this posterior requires having a latent target z for x . To this end, we use our decoder g_ϕ to create a target for x by first mapping x to a latent code z , then sampling from $g_\phi(z)$, and subsequently re-mapping this reconstruction back in the z -space. We summarize this procedure in Figure 2.

As in [17], $f(\cdot; \eta)$ plays a role analogous to q_ψ in eq. (1). It gives us means to sample latent codes from a particle θ_m given an input x without imposing an explicit and functional parametric form for q_ψ . Unlike [17], we do not apply SVGD on the latent codes but on the particles that generate the codes. By also being Bayesian, every particle θ_m provides some prior information $p(\theta_m)$ on how to sample these codes. During training and inference, we use bayesian model averaging across the particles outputs to get a latent code z from x ; formally, if $x \in \mathcal{D}$, for instance, then $z \sim p(z|x; \mathcal{D})$ where the posterior p is given by:

$$p(z|x, \mathcal{D}) = \int p(z|x, \theta) p(\theta|\mathcal{D}) d\theta \approx \frac{1}{M} \sum_{m=1}^M p(z|x, \theta_m).$$

4.2 Learning to Perturb a Manifold

Previously, we described a method to project \mathcal{D} in its embedding space to learn its manifold \mathcal{M} . In this section, we focus on learning to perturb the points of \mathcal{M} . We especially require the perturbed points to reside in \mathcal{M} so that they too exhibit the features of \mathcal{M} . Intuitively, we aim to learn a set of transformations³ Θ' that \mathcal{M} is *invariant to* or that preserve \mathcal{M} . Formally, if we let θ' be one such transformation, for instance, θ' must satisfy: $\forall v \in \mathcal{M}, \theta'(v) \in \mathcal{M}$.

Gram-Schmidt Gradient Sign Method (GGSM) is a new perturbation method we introduce – similar in spirit to fast-gradient sign method of [10] – to perturb the manifold \mathcal{M} . With GGSM, we want to render \mathcal{M} *invariant* to the perturbations induced by the transformations Θ' . In algebraic terms, if \mathbf{Z} is a subspace of \mathcal{M} , and \mathbf{U} an orthonormal basis of \mathbf{Z} , we perturb \mathbf{Z} by finding a subspace spanned by \mathbf{U} in the form of:

$$\text{span}(\mathbf{U}) = \left\{ \sum_{i=1}^{|\mathbf{U}|} \lambda_i u_i \mid u_i \in \mathbf{U}, \lambda_i \in \mathbb{R} \right\};$$

the goal being to get the values λ_i be as small as possible.

To start, let us define $\Theta' = \{\theta'_m\}_{m=1}^M$ where every θ'_m defines the weights and biases of a Bayesian neural network. Let \mathcal{B}_x be a minibatch of training samples of \mathcal{D} , and \mathcal{B}_z^m be their latent codes where for every $z_{im} \in \mathcal{B}_z^m$, $z_{im} \sim p(z|x_i, \theta_m)$ with $x_i \in \mathcal{B}_x$. We aim to learn each $\theta'_m \in \Theta'$ in a way to

³The reason why we maintain new model instances stems from the need – we expressed in Definition 1.2 – to find some points v that lie in the close vicinity of a point u in the z -space.

generate perturbed versions of \mathcal{B}_z^m along the directions of an orthonormal basis \mathbf{U}_m . Given that a manifold is locally Euclidean, we measure the dimension of a local neighborhood of \mathcal{B}_z^m by applying Gram-Schmidt to orthogonalize the span of representative local points. We formalize this objective as an optimization problem where we jointly learn the perturbations λ_m and the directions $\text{sign}(\mathbf{U}_m)$ along which we should perturb \mathcal{B}_z^m . More specifically, we consider the following update rules:

$$\begin{aligned} \lambda_m &\leftarrow \lambda_m - \alpha \nabla_{\lambda_m} \tau'(\lambda_m, \theta'_m); \theta'_m \leftarrow \theta'_m - \alpha \nabla_{\theta'_m} \tau'(\lambda_m, \theta'_m) \text{ with} \\ \tau'(\lambda_m, \theta'_m) &= \sum_{x_i, z_i} \left\| z'_{im} - [z_{im} + \lambda_m \odot \text{sign}(u_{im})] \right\|_2^2 \\ \text{where } z'_{im} &\sim p(z'|x, \theta'_m), u_{im} = z_{im} - \sum_{j=1}^{i-1} \text{proj}_{u_{jm}}(z_{im}) \text{ and } \text{proj}_{u_j}(z_i) = \frac{\langle u_j, z_i \rangle}{\|u_j\|_2^2} u_j \end{aligned} \quad (5)$$

To further describe the update rules in eq. (5), we first sample a model instance θ'_m from $f(\xi_m; \eta')$, then we generate M latent codes $z'_{im} \sim p(z'|x_i, \theta'_m)$ with $x_i \in \mathcal{B}_x$. We compute an orthonormal basis \mathbf{U}_m for \mathcal{B}_z^m and optimize for the noise tensor λ_m that minimizes the objective τ' along the directions of the basis vectors $u_i^m \in \mathbf{U}_m$. With λ_m fixed, we minimize τ' again to get θ'_m .

For large M , maintaining Θ' can however be computationally prohibitive. Thus, as in section 4.1, we make use of a recognition network $f(\cdot; \eta')$ that takes as input some noise $\xi'_m \sim \mathcal{N}(0, I)$ and generates $\theta'_m = f(\xi'_m; \eta')$. As before, η' is here too updated through a small number of gradient steps; that is at iteration $j+1$, we get η'^{j+1} by:

$$\eta'^{j+1} \leftarrow \underset{\eta'}{\text{argmin}} \sum_{m=1}^M \left\| \underbrace{f(\xi'_m; \eta'^j)}_{\theta_m'^j} - \theta_m'^{j+1} \right\|_2^2 \quad \text{where } \theta_m'^{j+1} \leftarrow \theta_m'^j - \alpha \nabla_{\theta_m'^j} \tau'(\lambda_m, \theta_m'^j) \quad (6)$$

In the following, we use the notation $\text{GGSM}(\Theta', \lambda)$ where $\lambda = [\lambda_1, \dots, \lambda_M]^\top$ to update Θ' .

Distribution Matching - Although GGSM confers us clear benefits in the forms of latent noise imperceptibility and sampling speed, it cannot prevent the model instances Θ' from deviating from the particles Θ . This understandably contradicts the requirement in Definition 1.2 that the discrepancy between ω_1 and ω_2 , $\mathcal{D}_f(\omega_1 \| \omega_2)$ – in this context Θ and Θ' – to be as minimal as possible so as to render the dissimilarity between adversarial samples we generate afterwards and real inputs as imperceptible as possible. To remedy this, we further regularize the $\theta'_m \in \Theta'$ after every GGSM update. In essence, we apply one SVGD update on the θ'_m 's. Unlike in eq. (2), the parameters Θ' determine here their own update direction by consulting the particles Θ alone instead of consulting each other. We slightly modify the objective τ in eq. (2) to ensure the model instances $\theta' \in \Theta'$ follow the transform maps constructed by the $\theta \in \Theta$ [18]:

$$\theta'_{t+1} \leftarrow \theta'_t + \epsilon'_t \tilde{\tau}(\theta'_t) \text{ where } \tilde{\tau}(\theta'_t) = \frac{1}{M} \sum_{j=1}^M \left[k(\theta'_t, \theta_t^j) \nabla_{\theta'_t} \log p(\theta_t^j) + \nabla_{\theta'_t} k(\theta'_t, \theta_t^j) \right]. \quad (7)$$

In the following, we use $\text{SVGD}_{\tilde{\tau}}$ to denote the gradient update rule in eq. (7) using the operator $\tilde{\tau}$.

4.3 Jointly Learning to Project and Attack

To introduce our approach, we decomposed the adversarial learning problem into two tasks: 1) manifold learning where we introduced a new method to project high-dimensional data into a low dense representation to faithfully characterize its distribution, and 2) manifold perturbation where we ensure cases we perturb remain in the manifold of the true examples. Here, we show how both tasks can be unified in one learning procedure to generate adversarial examples.

In general, there are two ways to produce adversarial examples: via white-box [10] or black-box [19] attack. In the more standard black-box case, which is the main focus of this study, we only have access to the predictions of a classifier g and need to produce adversaries not knowing the intricacies of g nor having access to its loss function. In this setting, adversarial examples are produced by maximizing an auxiliary loss, here the log-likelihood $P(y'|x')$, of a target class $y' \in \mathcal{Y} \setminus \{y\}$ over an ϵ -radius ball around the input x [14]. This is formalized as:

$$x' = \underset{x': \|x' - x\|_p \leq \epsilon_{\text{attack}}}{\text{argmax}} \log P(y'|x'). \quad (8)$$

Algorithm 1 Project and attack. $d = \|\cdot\|_2$ is the distance.

Require: $(x, y) \in \mathcal{D} \times \mathcal{Y}, M, g, \beta, \beta'$
Initialize $\eta, \eta', \lambda = [\lambda_1, \dots, \lambda_M]^\top, \xi = [\xi_1, \dots, \xi_M]^\top$
for $i = 1$ **to** inner-gradient-updates **do**
 Compute $\Theta = \{\theta_m\}_{m=1}^M$ where $\theta_m = f_\eta(\xi_m)$
 Compute $\Theta' = \{\theta'_m\}_{m=1}^M$ where $\theta'_m = f_{\eta'}(\xi_m)$
 Sample z and z' using Θ and Θ' respectively
 Sample \tilde{x} and x' from g_ϕ with inputs z and z'
 if $i > 1$ **then**
 $\eta \leftarrow \eta - \beta \nabla_\eta d(\Theta(\eta), \text{SVGD}_\tau(\Theta(\eta)))$ # via inverting \tilde{x}
 $\lambda, \Theta'(\eta') \leftarrow \text{GGSM}(\Theta'(\eta'), \lambda)$
 $\eta' \leftarrow \eta' - \beta' \nabla_{\eta'} d(\Theta'(\eta'), \text{SVGD}_{\tilde{\tau}}(\Theta'(\eta')))$
 end if
end for
 Use x' in loss \mathcal{L} in eq. (9) and propagate back its gradient.

Thus, given g , we illustrate this end-to-end procedure in algorithm 1. First, we sample Θ , the particles that learn to model the distribution of \mathcal{D} in its manifold \mathcal{M} , from f_η . Then, we sample Θ' , a set of transformations from $f_{\eta'}$ we want \mathcal{M} to be invariant to under the perturbations these transformations induce. Both Θ and Θ' act as encoders of \mathcal{D} but Θ more faithfully than Θ' . Both also attempt to capture the complex uncertainty structure of \mathcal{D} by learning to approximate its predictive posterior in eq. (3). To optimize Θ , we have to compute this posterior. We do so after the first inner gradient update by using the inversion mechanism we described in Figure 2 in an iterative fashion. From updating Θ , we optimize f_η using stochastic gradient descent. Then, we apply τ' in eq. (7) to optimize Θ' , and subsequently update η' . This summarizes the inner-training of the recognition networks f_η and $f_{\eta'}$. To generate adversarial examples, we extend the objective in eq. (8) as follows:

$$\mathcal{L} = \mathcal{L}_{\text{rec}} + \min_{y' \in \mathcal{Y}} \left[\mathbb{1}_{y=y'} \cdot \log(1 - P(y'|x')) \right], \quad (9)$$

where \mathcal{L}_{rec} is the reconstruction error of x that we formalize in section 5; the second term is the cost incurred for failing to fool the classifier g . Notice that we did not require in Definition 1.2 the constraint $\|x - x'\|_p \leq \epsilon_{\text{attack}}$ to hold. However, for the purpose of targeting the certified defenses [4] and [6], we enforce the constraint during training and stop when it is satisfied.

5 Experiments & Results

We evaluate our approach on a number of black-box classification tasks of images and text.

Image Datasets - For image classification, we experiment with three standard datasets: MNIST [20], CelebA [21] and SVHN [22]. For MNIST and SVHN, each image of a digit represents the class the image belongs to. For CelebA, we group the face images according to their gender (female, male), and focus on gender classification similar to [2].

Text Datasets - For text classification, we consider the SNLI [23] dataset. SNLI consists of sentence pairs where each pair contains a premise and a hypothesis, and a label indicating the relationship (*entailment*, *neutral*, *contradiction*) between the premise and hypothesis. For instance, the following pair is assigned the label *entailment* to indicate that the premise entails the hypothesis.

Premise: A soccer game with multiple males playing. Hypothesis: Some men are playing a sport.

Model Settings - We embed the image and text inputs using a convolutional neural network (CNN). To generate adversarial images, we design the decoder g_ϕ as a transpose CNN. For adversarial text generation, we consider two designs for g_ϕ : 1) a transpose CNN, and 2) a language model. The recognition networks f_η and $f_{\eta'}$ are fully connected neural networks of similar architecture. To evaluate our approach, we target a range of adversarial models. For more details on the architectures of these models, the CNN embedder, f_η , $f_{\eta'}$, and the decoder g_ϕ , we refer the reader to appendix A.

Table 1: Adversarial success rates (%) against MNIST, CelebA, and SVHN ResNet models; and also for MNIST against certified defenses [4][†] and [6][‡] respectively.

	Adv. MNIST	ResNet CelebA (adv.)	ResNet SVHN (adv.)
Latent noise levels	0.004± 0.0003	0.033± 0.008	0.033± 0.008
Non-certified defense	97.2	84.4	87.6
Certified defenses	95.2 [†] 96.8 [‡]	-	-

Table 2: Test samples and adversarial hypotheses for scenario 1.

True Input 1	<i>Premise:</i> A person is riding a bike. <i>Hypothesis:</i> A biker races. <i>Label:</i> Entailment
Adversary 1	<i>Hypothesis:</i> A man races. <i>Label:</i> Contradiction
True Input 2	<i>Premise:</i> Girls walk down the street. <i>Hypothesis:</i> The girls walk down the street. <i>Label:</i> Entailment
Adversary 2	<i>Hypothesis:</i> A choir walks down the street. <i>Label:</i> Neutral
True Input 3	<i>Premise:</i> Two children surf. <i>Hypothesis:</i> Two kids in blue wetsuits surf. <i>Label:</i> Entailment
Adversary 3	<i>Hypothesis:</i> Two kids in a lift. <i>Label:</i> Contradiction
True Input 4	<i>Premise:</i> Two puppies play with a red ball. <i>Hypothesis:</i> Two dogs playing fetch. <i>Label:</i> Neutral
Adversary 4	<i>Hypothesis:</i> Two people play in the snow. <i>Label:</i> Contradiction

5.1 Generating Image Adversaries

Setup - As argued in [1], the strongest non-certified defense to date against adversarial attacks is adversarial training with Projected Gradient Descent (PGD) [5]. We evaluate the strength of our MNIST, CelebA and SVHN adversaries against adversarially trained ResNet [24] models with a 40-step PGD and noise margin ϵ_{attack} less than 0.3. The ResNet models follow the architecture design of [2]. For MNIST, we also target two pre-trained certified defenses [4] and [6] with ϵ_{attack} set to 0.1.

We formalize \mathcal{L}_{rec} in eq. (9) respectively as two p -norm losses and a *discriminative* loss. For the p -norm case, we first reconstruct using the true inputs as targets, i.e., $\mathcal{L}_{\text{rec}} = \|x - x'\|_p$ where $x \in \mathcal{D}$ and x' are samples we generate. For the latter, we use a pre-trained Wasserstein formulation of AC-GAN [25] to generate samples \hat{x} and set $\mathcal{L}_{\text{rec}} = \|\hat{x} - x'\|_p$. Finally, we use the discriminator of the same GAN to discriminate between x and x' . We experiment with all these \mathcal{L}_{rec} variants and report only the results where both the *adversarial success rates* and *sample quality* are high.

Adversarial Success Rate (ASR) - In Table 1, we report our best results both for the certified and non-certified target models. Against the non-certified defenses, we achieve an ASR of 97.2% for MNIST, 87.6% for SVHN, and 84.4% for CelebA. The certified defenses on MNIST guarantee that no attack with $\epsilon_{\text{attack}} \leq 0.1$ can have a success rate larger than 35% and 5.8% respectively. However, our ASR against these defenses is 95.2% and 96.8%. For all the datasets, the latent noise levels are smaller than ϵ_{attack} , and the accuracies of the target models are higher than 96.3%; thus proving the effectiveness of our method in generating strong adversaries.

Noise Level - We compute the latent strength of the adversaries by evaluating the average spectral norm of the learned perturbations over few minibatch samples. As can be noted in Table 1, the latent nuisances are smaller than ϵ_{attack} , and significantly lower than in [2]⁴. Beyond the imperceptibility of our adversaries, these noise levels show that the distributions the particles Θ and the model instances Θ' follow are similar. This is further illustrated in Figure 4 by the overlapping marginal distributions of Θ and Θ' ; thus resulting in good sample quality as exemplified in Figure 3.

5.2 Generating Text Adversaries

Setup - We perturb the hypotheses sentences to attack our SNLI classifier with the premise sentences kept unchanged. We use ARAE [26], similar to [12], for word embedding, and a CNN for sentence embedding. To generate sentences from the perturbed latent codes, we evaluate two scenarios where: 1) the decoder g_ϕ is a transpose CNN, and 2) g_ϕ is a language model. We detail the configuration

⁴Note that our results are not directly comparable with Song et al. [2] as their reported success rates are for targeted unrestricted adversaries computed using Amazon MTurkers votes.



Figure 3: Minibatches of images and all their adversarial examples (in red for CelebA).

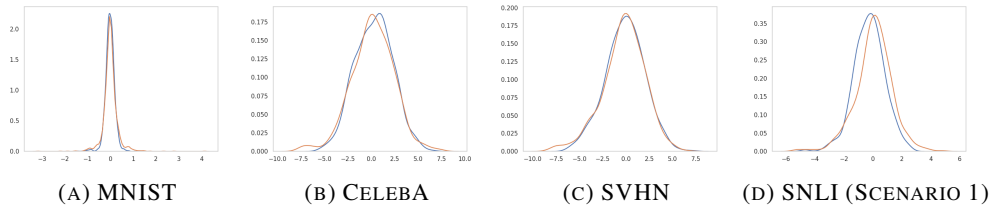


Figure 4: KDE plots: Marginal distributions on a test minibatch.

design of these architectures in appendix A. We formalize the reconstruction loss \mathcal{L}_{rec} in eq. (9) as a cross-entropy loss. We report our results, achieved with $M = 5$, in Table 2 and discuss them next.

Adversarial Success Rate (ASR) - In scenario 1, we achieve an ASR of 67.28% on the SNLI classifier with a test accuracy of 89.42%. In scenario 2, we obtain an ASR rate of 65.2%.

Noise Level - In adversarial text generation, small perturbations can go unnoticed in the outputs whereas high nuisances can render the outputs illegible or uninformative. We generate our text adversaries at word level using a vocabulary of 11,000 words only. As a result, for scenario 1, the

adversarial hypotheses and the premises look quite similar despite the differences in their vector representations. This can be explained by conditioning the generation on the premises and how small the learned nuisances are. We do not report the text adversaries for scenario 2 as most of the generated samples are not legible. We posit that this is due to the compounding effect of the perturbations on the language model. As future work, we will investigate other approaches like [26] and [27].

6 Related Work

Szegedy et al. [9] first demonstrated that deep neural networks could achieve high accuracy on previously unseen examples while being vulnerable to small adversarial perturbations. This finding has sparked keen interest in the research community to probe deep learning models [14, 1, 8, 10] in hope of understanding their weaknesses and to mitigate their vulnerabilities [3, 4, 5, 6]. Several studies have followed suit since then to improve the robustness of neural networks [3, 28].

In general, studies in adversarial deep learning can be categorized into two groups. The first group proposes to generate adversaries directly in the input data space by adding distortions, occlusions or changing illumination in input images [14, 29, 7] to cause changes in classification. Closer to our work is the second group which uses generative models [2, 12] to search for adversaries in the dense and continuous representation of the data rather than in its input space. The former proposals focus at perturbing images with noise or patterns that do not necessarily look realistic but that nonetheless can cause the images to be misclassified. The latter favor generating better looking, more natural and realistic adversarial examples.

Adversarial Images - Song et al. [2] propose to construct unrestricted adversarial examples by training a conditional generative model that constrains the search region for a z' in the neighborhood of a target z . Zhao et al. [12] propose mapping input images to a latent space using GANs, and to search for adversarial examples in that space. Both [12] and [2] studies are closely related to ours. However, in our case, we do not need to set the noise level to inject to the true inputs or their latent representations as the perturbations are automatically learned during training. Furthermore, by capturing the uncertainty induced by the mapping of the data to latent space, we learn to characterize the structure of the data better, which allows us to generate more realistic-looking adversaries.

Adversarial Text - Previous studies on adversarial text generation [26, 30, 31, 32] perform word erasures and replacements directly on the input space, using domain-specific rules or heuristics, or require manual curation. Recently, [12] propose to search for textual adversaries in the latent representation of the data. Our approaches are similar. However, the search for adversaries is handled more gracefully in our case thanks to an efficient gradient-based optimization method in lieu of a computationally expensive search in the latent space.

7 Conclusion

Many adversarial learning approaches usually fail to enforce the semantic-relatedness that ought to exist between true inputs and their adversaries. Motivated by this fact, we provided an approach tailored explicitly to ensuring that the adversaries and their inputs exhibit the same high-level characteristics and semantic features.

In summary, we proposed to construct adversarial examples from learning the manifold of the inputs. We developed a method to find adversaries of image and text inputs from within an input's own manifold by automatically learning to perturb its latent code with efficiently sampled and imperceptible noise. The resulting adversaries appear realistic, diverse, informative, and perceptually similar to the inputs.

References

- [1] Anish Athalye, Nicholas Carlini, and David A. Wagner. Obfuscated gradients give a false sense of security: Circumventing defenses to adversarial examples. *CoRR*, abs/1802.00420, 2018.
- [2] Yang Song, Rui Shu, Nate Kushman, and Stefano Ermon. Constructing unrestricted adversarial examples with generative models. In *Advances in Neural Information Processing Systems*

- 31: *Annual Conference on Neural Information Processing Systems 2018, NeurIPS 2018*, 3-8 December 2018, Montréal, Canada., pages 8322–8333, 2018.
- [3] Aman Sinha, Hongseok Namkoong, and John Duchi. Certifiable distributional robustness with principled adversarial training. In *International Conference on Learning Representations*, 2018.
 - [4] Aditi Raghunathan, Jacob Steinhardt, and Percy Liang. Certified defenses against adversarial examples. *CoRR*, abs/1801.09344, 2018.
 - [5] Aleksander Madry, Aleksandar Makelov, Ludwig Schmidt, Dimitris Tsipras, and Adrian Vladu. Towards deep learning models resistant to adversarial attacks. *CoRR*, abs/1706.06083, 2017.
 - [6] J. Zico Kolter and Eric Wong. Provable defenses against adversarial examples via the convex outer adversarial polytope. *CoRR*, abs/1711.00851, 2017.
 - [7] Nicholas Carlini and David A. Wagner. Towards evaluating the robustness of neural networks. *CoRR*, abs/1608.04644, 2016.
 - [8] Alexey Kurakin, Ian J. Goodfellow, and Samy Bengio. Adversarial examples in the physical world. *CoRR*, abs/1607.02533, 2016.
 - [9] Christian Szegedy, Wojciech Zaremba, Ilya Sutskever, Joan Bruna, Dumitru Erhan, Ian Goodfellow, and Rob Fergus. Intriguing properties of neural networks. In *International Conference on Learning Representations*, 2014.
 - [10] Ian J. Goodfellow, Jonathon Shlens, and Christian Szegedy. Explaining and harvesting adversarial examples. *CoRR abs/1412.6572*, 2014.
 - [11] Diederik P. Kingma and Max Welling. Auto-encoding variational bayes. *International Conference on Learning Representations (ICLR)*, 2014.
 - [12] Zhengli Zhao, Dheeru Dua, and Sameer Singh. Generating natural adversarial examples. In *International Conference on Learning Representations*, 2018.
 - [13] Uri Shaham, Yutaro Yamada, and Sahand Negahban. Understanding adversarial training: Increasing local stability of supervised models through robust optimization. *Neurocomputing*, 307:195–204, 2018.
 - [14] Anish Athalye, Logan Engstrom, Andrew Ilyas, and Kevin Kwok. Synthesizing robust adversarial examples. *CoRR*, abs/1707.07397, 2017.
 - [15] Qiang Liu and Dilin Wang. Stein variational gradient descent: A general purpose Bayesian inference algorithm. *Neural Information Processing Systems (NIPS)*, 2016.
 - [16] Shengjia Zhao, Jiaming Song, and Stefano Ermon. InfoVAE: Information maximizing variational autoencoders. *CoRR*, abs/1706.02262, 2017.
 - [17] Yunchen Pu, Zhe Gan, Ricardo Henao, Chunyuan Li, Shaobo Han, and Lawrence Carin. VAE learning via Stein variational gradient descent. *Neural Information Processing Systems (NIPS)*, 2017.
 - [18] Jun Han and Qiang Liu. Stein variational adaptive importance sampling. *Conference on Uncertainty in Artificial Intelligence (UAI)*, 2017.
 - [19] Nicolas Papernot, Patrick McDaniel, Ian Goodfellow, Somesh Jha, Z. Berkay Celik, and Ananthram Swami. Practical black-box attacks against machine learning. In *Proceedings of the 2017 ACM on Asia Conference on Computer and Communications Security*, ASIA CCS ’17, pages 506–519, New York, NY, USA, 2017. ACM.
 - [20] Y. LeCun, B. Boser, J. S. Denker, D. Henderson, R. E. Howard, W. Hubbard, and L. D. Jackel. Backpropagation applied to handwritten zip code recognition. *Neural Comput.*, 1(4):541–551, December 1989.
 - [21] Ziwei Liu, Ping Luo, Xiaogang Wang, and Xiaoou Tang. Deep learning face attributes in the wild. In *Proceedings of International Conference on Computer Vision (ICCV)*, December 2015.
 - [22] Yuval Netzer, Tao Wang, Adam Coates, Alessandro Bissacco, Bo Wu, and Andrew Y. Ng. Reading digits in natural images with unsupervised feature learning. In *NIPS Workshop on Deep Learning and Unsupervised Feature Learning 2011*, 2011.
 - [23] Samuel R. Bowman, Gabor Angeli, Christopher Potts, and Christopher D. Manning. A large annotated corpus for learning natural language inference. *CoRR*, abs/1508.05326, 2015.

- [24] Kaiming He, Xiangyu Zhang, Shaoqing Ren, and Jian Sun. Deep residual learning for image recognition. *CoRR*, abs/1512.03385, 2015.
- [25] Augustus Odena, Christopher Olah, and Jonathon Shlens. Conditional image synthesis with auxiliary classifier GANs. In Doina Precup and Yee Whye Teh, editors, *Proceedings of the 34th International Conference on Machine Learning*, volume 70 of *Proceedings of Machine Learning Research*, pages 2642–2651, International Convention Centre, Sydney, Australia, 06–11 Aug 2017. PMLR.
- [26] Junbo Zhao, Yoon Kim, Kelly Zhang, Alexander Rush, and Yann LeCun. Adversarially regularized autoencoders. In Jennifer Dy and Andreas Krause, editors, *Proceedings of the 35th International Conference on Machine Learning*, volume 80 of *Proceedings of Machine Learning Research*, pages 5902–5911, Stockholmsmssan, Stockholm Sweden, 10–15 Jul 2018. PMLR.
- [27] Sandeep Subramanian, Sai Rajeswar Mudumba, Alessandro Sordoni, Adam Trischler, Aaron Courville, and Christopher Pal. Towards text generation with adversarially learned neural outlines. In *Advances in Neural Information Processing Systems*, volume 31, 2018.
- [28] Nicolas Papernot, Patrick D. McDaniel, Xi Wu, Somesh Jha, and Ananthram Swami. Distillation as a defense to adversarial perturbations against deep neural networks. *CoRR*, abs/1511.04508, 2015.
- [29] Seyed-Mohsen Moosavi-Dezfooli, Alhussein Fawzi, Omar Fawzi, and Pascal Frossard. Universal adversarial perturbations. *CoRR*, abs/1610.08401, 2016.
- [30] Robin Jia and Percy Liang. Adversarial examples for evaluating reading comprehension systems. *CoRR*, abs/1707.07328, 2017.
- [31] David Alvarez-Melis and Tommi S. Jaakkola. A causal framework for explaining the predictions of black-box sequence-to-sequence models. *CoRR*, abs/1707.01943, 2017.
- [32] Jiwei Li, Will Monroe, and Dan Jurafsky. Understanding neural networks through representation erasure. *CoRR*, abs/1612.08220, 2016.

Appendix A: Detailed Experimental Settings

Table 3: ResNet Classifier.

	Configuration	Replicate Block
Initial Layer	3×3 conv. m maps. 1×1 stride.	-
Residual Block 1	batch normalization, leaky relu 3×3 conv. m maps 1×1 stride batch normalization, leaky relu 3×3 conv. m maps. 1×1 stride residual addition	$\times 10$
Residual Block 1	batch normalization, leaky relu 3×3 conv. $2m$ maps 2×2 stride batch normalization, leaky relu 3×3 conv. $2m$ maps. 1×1 stride average pooling, padding	-
Residual Block 2	batch normalization, leaky relu 3×3 conv. $2m$ maps 2×2 stride batch normalization, leaky relu 3×3 conv. $2m$ maps. 1×1 stride average pooling, padding	$\times 9$
Residual Block 2	batch normalization, leaky relu 3×3 conv. $2m$ maps 2×2 stride batch normalization, leaky relu 3×3 conv. $2m$ maps. 1×1 stride average pooling, padding	-
Residual Block 3	batch normalization, leaky relu 3×3 conv. $2m$ maps 2×2 stride batch normalization, leaky relu 3×3 conv. $2m$ maps. 1×1 stride average pooling, padding	$\times 9$
Pooling Layer	3×3 conv. m maps. 1×1 stride.	-
Output Layer	3×3 conv. m maps. 1×1 stride.	-

Table 4: Model Configurations + SNLI Classifier + Hyper-parameters.

	Name	Configuration
Recognition Networks	f_η	Input Dim: 50, Hidden Layers: [60, 70], Output Dim: Num weights & biases in θ_m
	f'_η	Input Dim: 50, Hidden Layers: [60, 70], Output Dim: Num weights & biases in θ'_m
Model Instances	Particles θ_m	Input Dim: 28×28 (MNIST), 64×64 (CelebA), 32×32 (SVHN), 300 (SNLI) Hidden Layers: [40, 40] Output Dim (latent code): 100
	Parameters θ'_m	Input Dim: 28×28 (MNIST), 64×64 (CelebA), 32×32 (SVHN), 100 (SNLI) Hidden Layers: [40, 40] Output Dim (latent code): 100
Feature Extractor		Input Dim: $28 \times 28 \times 1$ (MNIST), $64 \times 64 \times 3$ (CelebA), $32 \times 32 \times 3$ (SVHN), 10×100 (SNLI) Hidden Layers: [40, 40] Output Dim: 28×28 (MNIST), 64×64 (CelebA), 32×32 (SVHN), 100 (SNLI)
Decoder	Transpose Conv. Net	For CelebA & SVHN: [filters: 64, stride: 2, kernel: 5] $\times 3$ For SNLI: [filters: 64, stride: 1, kernel: 5] $\times 3$
	Language Model	Vocabulary Size: 11,000 words Max Sentence Length: 10 words -
SNLI classifier		Input Dim: 200, Hidden Layers: [100, 100, 100], Output Dim: 3
Learning Rates	Adam Optimizer ($\alpha = 10^{-3}$), $\beta = 10^{-2}$, $\beta' = 10^{-2}$	
More settings	Batch size: 64, Inner-updates: 3, Training epochs: 500	

Appendix B: Additional Results

Table 5: More examples of adversarially generated hypotheses with the true premises kept unchanged.

TRUE INPUT 1	<i>Premise:</i> A person is riding a bike. Hypothesis: A BIKER RACES <i>Label:</i> ENTAILMENT
ADVERSARY	Hypothesis: A MAN RACES. <i>Label:</i> CONTRADICTION
TRUE INPUT 2	<i>Premise:</i> Girls walk down the street Hypothesis: THE GIRLS WALK DOWN THE STREET <i>Label:</i> ENTAILMENT
ADVERSARY	Hypothesis: A CHOIR WALKS DOWN THE STREET. <i>Label:</i> NEUTRAL
TRUE INPUT 3	<i>Premise:</i> Two wrestlers are competing and are brothers. Hypothesis: TWO WRESTLERS IN AN INTENSE MATCH. <i>Label:</i> NEUTRAL
ADVERSARY	Hypothesis: TWO WOMEN ARE PLAYING TOGETHER. <i>Label:</i> CONTRADICTION
TRUE INPUT 4	<i>Premise:</i> A group of people celebrate. Hypothesis: A GROUP OF PEOPLE CELEBRATE THEIR ASIAN CULTURE. <i>Label:</i> ENTAILMENT
ADVERSARY	Hypothesis: A GROUP OF PEOPLE CRUISING IN THE WATER. <i>Label:</i> NEUTRAL
TRUE INPUT 5	<i>Premise:</i> Cheerleaders are wearing outside. Hypothesis: CHEERLEADERS STANDING ON A FOOTBALL FIELD. <i>Label:</i> ENTAILMENT
ADVERSARY	Hypothesis: PERSON STANDING ON A PLAYING FIELD. <i>Label:</i> NEUTRAL
TRUE INPUT 6	<i>Premise:</i> Two children surf. Hypothesis: TWO KIDS IN BLUE WETSUITS SURF. <i>Label:</i> ENTAILMENT
ADVERSARY	Hypothesis: TWO KIDS IN A LIFT. <i>Label:</i> CONTRADICTION
TRUE INPUT 7	<i>Premise:</i> People are eating in this picture'. Hypothesis: PEOPLE ARE ENJOYING FOOD AT A CROWDED RESTAURANT. <i>Label:</i> ENTAILMENT
ADVERSARY	Hypothesis: PEOPLE ARE ENJOYING LOOKING AT A CROWDED RESTAURANT. <i>Label:</i> CONTRADICTION

Table 6: Comparison between CelebA test samples and their adversaries.

TEST INPUTS	ADVERSARIES
	
	
	

Table 7: Comparison between SVHN images and their adversaries. Images in the Adversaries column are all adversarial.






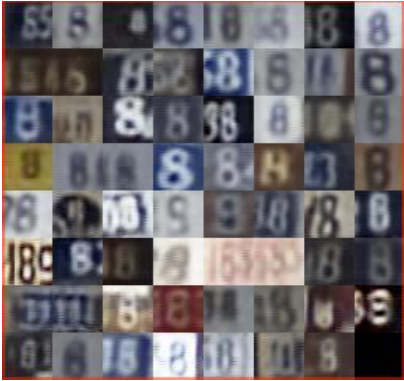
TEST INPUTS	ADVERSARIES
	
	
	

Table 8: Comparison between MNIST test samples and their adversaries.

TEST INPUTS	ADVERSARIES